Surface structure and stability of partially

hydroxylated silica surfaces

3

1

2

J.M. Rimsza¹, R.E. Jones², and L.J. Criscenti¹

5

- ¹Geochemistry Department, Sandia National Laboratories, Albuquerque, New Mexico 87185
- 7 USA
- 8 ²Science-Based Material Modeling Department, Sandia National Laboratories, Livermore, CA
- 9 94551 USA

10 11

12

13 14

15

16

17

18

19

20

21

22

23

24

25

26

27

28

29

30

Abstract

Surface energies of silicates influence crack propagation during brittle fracture and decrease with surface relaxation caused by annealing and hydroxylation. Molecular-level simulations are particularly suited to investigating surface processes. In this work, classical molecular dynamics (MD) simulations of silica surfaces with a non-reactive ClayFF forcefield and the reactive bond-order based forcefield ReaxFF are performed to investigate the effect of forcefield reactivity on surface structure and energy through surface relaxation and interaction with ambient water. Unhydroxylated fracture surface energies of 5.1 J/m² are calculated with the ClayFF forcefield and 2.0 J/m² for the ReaxFF forcefield. The ClayFF surface energies are consistent with the experimental results from double cantilever beam fracture tests (4.5 J/m²), while ReaxFF underestimated these surface energies. Surface relaxation via hydroxylation and annealing was performed creating a low energy equilibrium surface. Annealing condensed neighboring siloxane bonds, increased surface connectivity, and decreased the surface energies by 0.2 J/m² for ClayFF and 0.8 J/m² for ReaxFF. Post-hydroxylation surfaces energies decreased further to 4.6 J/m² with the ClayFF forcefield and 0.2 J/m² with the ReaxFF forcefield. Experimental equilibrium surface energies are ~0.35 J/m², consistent with the ReaxFF forcefield. Although neither forcefield was capable of replicating both the fracture and equilibrium surface energies reported from experiment, each was consistent with one of these conditions. Therefore, future computational investigations that rely on accurate surface energy values should consider the surface state of the system and select the appropriate forcefield.

fluctuations as the crack propagates.

1. Introduction

The mechanical properties and fracture behavior of silica affects geological phenomena ¹⁻⁴, optical applications in glass fibers ⁵⁻⁶, and the use of silicates as sensors or absorbents ⁷⁻⁹. Silica fracture surfaces exhibit non-equilibrium structures and energies due to limited exposure to the environment as the crack propagates ¹⁰⁻¹¹. Brittle fracture of glasses exposed to humid or aqueous environments has been investigated using experimental methods ranging from macroscale mechanical tests using specimens of various specialized geometries to post-fracture electron microscopy ¹²⁻¹⁴. The investigation of the reactive processes inherent in fracture and in particular, simulations capable of giving molecular-level details, is a nascent line of inquiry. Here, we lay the groundwork for fundamental studies of this type.

During brittle fracture, high-energy densities form near the crack tip ¹⁵⁻¹⁷ which are dissipated either as thermal energy or stored in the reconstructed surface as the crack propagates.

Temperature fluctuations from heat dissipation have been calculated using the specific heat and density of the material, and estimates of the heat dissipation zone with temperature increases of up to 1000K have been reported ¹⁵. Experimental measurements of heat dissipation identified even higher temperature spikes up to 3200K during silica fracture by measuring radiation emissions ¹⁵. Such high temperature annealing can reform siloxane bonds on the silica surface through condensation of adjacent silanol species ¹⁸, altering the surface energy and reactivity. Local heat dissipation at crack tips can alter surface energies and structures, and in this work high temperature annealing simulates the relaxation of the surface due to temperature

Fracture toughness of silicates decreases in humid environments, due to surface site hydroxylation changing the surface energy at the crack tip $^{19\text{-}21}$. In the presence of water, the kinetics of molecular-scale crack infiltration can vary with pressure, humidity, temperature, and the phase of the water 22 . Silica crack propagation rates (v) in the presence of water are dependent on the diffusion coefficient of water in air (D_{H2O}), the partial pressure of the vapor phase in the atmosphere (p_{H2O}), and the crack velocity in a dry environment (ν_0) 22 .

$$v = v_o \cdot p_{H_2O} \cdot D_{H_2O} \tag{1}$$

When the crack velocity and water diffusion rate inside the crack are approximately equal, the concentration of water molecules at the crack tip drops, slowing crack propagation ²². With few

water molecules available to react with the surface, the hydroxylation rates decrease ¹⁰. Therefore, partial hydroxylation may occur for short time frames during crack propagation, altering the surface energy along the crack length. In this work both annealing, to simulate heat dissipation, and hydroxylation are included to create low energy equilibrium surfaces, calculate surface energies, and analyze surface structures.

From the 1970s to the present, a wide range of surface energies have been reported and vary with experimental method (Fig.1). Experimental measurements of silicate surface energies using double cantilever beam (DCB) fracture lie between 4.4-5.3 J/m², depending on the environment ²³⁻²⁵.

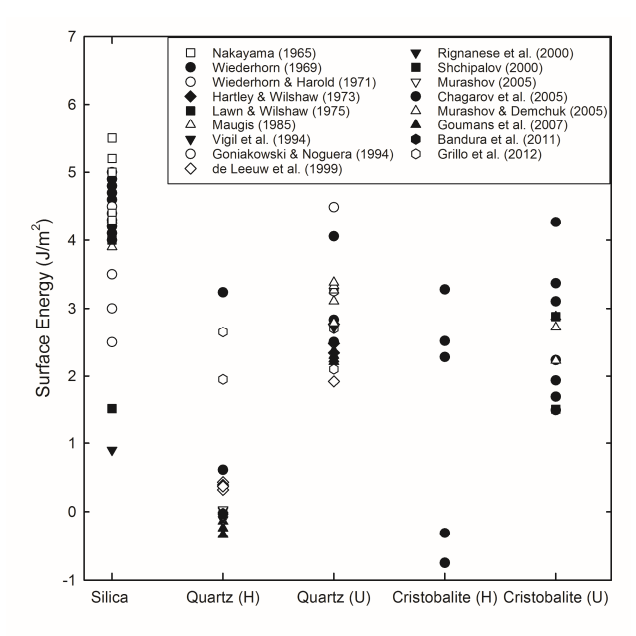


Figure 1: Surface energies for hydroxylated (H) and unhydroxylated (U) surfaces of silica polymorphs and amorphous silica. References: 19, 21, 23, 25-38

These fracture surface energies are significantly higher than equilibrium values (\sim 0.35 J/m²) of fully relaxed surfaces for several reasons ³⁹. Surface energies decrease during interaction with water, with a first drop due to hydroxylation, followed by further decreases with adsorption of a water monolayer, and then reaching a lowest energy value when in contact with bulk water ². An analytical expression for decreasing surface energy with environmental factors was put forth by Hammond and Ravitz: ⁴⁰.

$$\gamma_o - \gamma_v = \frac{RT}{MA} \int_0^P \frac{q}{p_{H_2}o} dp \tag{2}$$

with γ_v as the surface energy in a vacuum, γ_o as surface energy in vapor, R as the ideal gas constant, T as the temperature, M as the molecular weight of the vapor, A as the specific surface area of the solid (cm²/g), p_{H2O} as the pressure of the water vapor, and q as the grams of vapor absorbed per gram of solid. Using the above expression a drop in the quartz surface energy with saturation in water vapor was reported as ~0.24 J/m² from adsorption isotherms ⁴⁰. Experimental analysis of the fracture surface energies is complicated by the limited ability to control the environment at the crack tip ²², measurement of surface silanol concentrations ⁴¹, and fast relaxation kinetics of the surface ¹⁰.

Computational analysis of silicate fracture surface energies have focused on α -quartz, which develops ordered symmetric surfaces and are well suited to simulations. Unhydroxylated surface energies on α -quartz are between 1.9-2.8 J/m² for classical MD simulations, with the lowest value for the [0001] surface due to the reformation of four-coordinated silicon 27 . Hydroxylation decreases the surface energies to 0.3-0.4 J/m² with the higher concentration of isolated hydroxyls on the [1011] surface resulting in the lowest surface energy 27 . Density functional theory (DFT) simulations on the [0001] plane in α -quartz also resulted in decreases in surface energies with hydroxylation, with 2.21-2.37 J/m² reported for unhydroxylated surfaces and -0.14 J/m² to -0.34 J/m² after hydroxylation 28 . Additional computational studies on α -quartz $^{26,\,29-32}$ describe unhydroxylated surface energies between 1.96-2.11 J/m² with a few high values of 4.5-8.4 J/m² in simulations which did not include surface relaxation 32 .

Overall, simulation methods are capable of investigating the differences in surface energies between unhydroxylated and hydroxylated surface of quartz, but have yet to be extended to a systematic study of amorphous silica surfaces.

The particular classical MD forcefield affects silica surface structure and energy as well as controlling bulk and elastic properties of the system ⁴²⁻⁴³. The forcefield description of defect species, siloxane bond energies, hydroxyl group geometries, and water parameters alters the hydroxylated and unhydroxylated surface energies. Due to variations in forcefields, selection of a classical MD forcefield that accurately represents the surface structure and energy is critical in modeling silica fracture in aqueous environments. For example, reparametrization of the Si-O parameters in a classical MD forcefield by Du and de Leeuw resulted in an 8% decrease in the adsorption energy of disassociated water molecules ⁴⁴. Almost none of the currently available forcefields include surface properties in the parametrization, causing difficulty with accurately

simulating complex interfaces. Using forcefields with two different forms and level of reactivity, we investigate the role of interatomic forcefields play in the accuracy of the surface properties of silica.

The first forcefield is ClayFF, composed of Coulombic (E_{Coul}) and van der Waals (E_{VDW} , in the form of the Lennard-Jones potential) energy terms to describe the interatomic interactions together with harmonic bond (E_{bond}) and angle-stretching (E_{angle}) terms for surface hydroxyl groups ⁴⁵:

$$E_{total} = E_{Coul} + E_{VDW} + E_{bond} + E_{angle}$$
 (3)

- ClayFF was parametrized with simple oxides including quartz (α -SiO₂), hydroxides,
- oxyhydroxides, and kaolinite (Al₂Si₂O₅(OH)₄) bulk structures, and gas phase cluster models (
- Si(OH)₄) and Si(OH₂)₄⁴⁺) for the Si-O parameters. Water molecules in ClayFF are simulated
- using a non-reactive flexible simple point charge (SPC) water model with Lennard-Jones short
- range interactions ⁴⁵. ClayFF has been successfully applied to amorphous ⁴⁶⁻⁴⁷ and crystalline
- silicates⁴⁸ as well as on interactions between hydroxylated silica surfaces and water ⁴⁸⁻⁵¹.
- The second forcefield is ReaxFF, a bond-order based forcefield which allows for the
- breakage and formation of bonds during the simulation, with a complex total energy term ⁵²:
- $E_{Total} = E_{Bond} + E_{Over} + E_{Under} + E_{LP} + E_{Val} + E_{Pen} + E_{Tors} + E_{Conj} + E_{VDW} + E_{Coul}$ (4)
- The energy is a combination of bond energy (E_{bond}) , over-coordination energy penalty (E_{Over}) ,
- energy penalty to approximate unbonded Π -electrons (E_{Under}), energy of lone pairs (E_{LP}), valence
- angle energy term (E_{Val}), energy penalty to account for stable systems with double bonds (E_{Pen}),
- torsion angle energy term (E_{Tors}), conjugate components of the molecular energy (E_{Conj}), long
- range van der Waals interaction in the form of a distance corrected Morse potential (E_{VDW}), and a
- shielded columbic interaction $(E_{Coul})^{53}$. All ten energy terms smoothly approach zero as the
- interatomic distances increase to avoid discontinuities in energy ⁵³. Due to the complexities of
- the potential functions and the need to reevaluate bond orders at every time step, ReaxFF runs
- 138 10-50x slower compared with Lennard-Jones forcefields using analogous computational cells as
- benchmarked by Zheng, Li, and Guo ⁵⁴.

113

114

115

116

117

118

119

140

141

142

143

ReaxFF was first parametrized for silica-water systems by Fogarty et al.⁵⁵ using bond dissociation curves and distortions for Si/O/H structures, equations of states for bulk silica, and quantum mechanical data for binding and disassociation of water with Si(OH)₄ as well as Si(OH)₄ polymerization energies. ReaxFF also allows for variable partial atomic charges through

the charge equilibration (QEq) method and has been widely implemented in the investigation of water-silica interactions ^{52, 56-58}.

By comparing the surface properties of silica when simulated with the ClayFF and ReaxFF forcefield, future studies which rely heavily on the surface energies and structure of silica can make use of the forcefield which best represents the conditions of the system. This paper will evaluate the surface energy of amorphous silica using computational methods, validate the results with available experimental data, and connect differences in the surface structure with the structure of the forcefield. The detailed understanding of the effect of surface hydroxylation and annealing on surface energies provided by this study is crucial to further computational investigations of silica fracture and stress corrosion cracking.

2. Simulation Methods

To create silica surfaces, bulk silica simulation cells were created using a melt and quench procedure. A 3000 atom system with a 1:2 ratio of silicon and oxygen atoms was heated to 4000K and held for 100ps to melt the structure. The silica was then quenched from 4000K to 300K at a rate of 5K/ps with a 0.25fs and 1fs time step for the ReaxFF and ClayFF simulations respectively. A canonical ensemble controlled the density during both melting and quenching at 2.2 g/cm³, the experimental density of silica ⁵⁹. A Nosé-Hoover thermostat and barostat were used with 100 and 1000 time step damping parameters, respectively. Once the glass was quenched, a 100ps equilibration run was performed which allowed for pressure and density fluctuations through the use of an isothermal-isobaric (NPT) ensemble. Final silica densities were 2.26 g/cm³ for the ClayFF simulations and 2.20 g/cm³ for the ReaxFF simulations. All simulations with ClayFF or ReaxFF were performed using the LAMMPS MD code developed at Sandia National Laboratories ⁶⁰. For ReaxFF simulations, LAMMPS was used with the USER-REAXC package with the Yeon and van Duin Si/O/H ReaxFF parameterization ^{52, 57}.

Once the bulk silica was equilibrated, a vacuum gap equal to 3 times the size of the silica simulation cell was inserted in one dimension creating two silica surfaces. Annealing of the surface was performed to approximate energy dissipation during brittle fracture; numerical analysis by Rountree et al. ¹² predicted temperatures along the surface reach ~1000K, which was selected as the highest annealing temperature. Intermediate temperatures were also investigated (700K, 500K, 300K) and 0K was used as the control. During annealing the center third of the

simulation cell was frozen and the surface regions were heated to the annealing temperature, held for 200ps, and then cooled to 0K at a rate of 5K/ps. For data collection a final 100ps simulation was performed using an NVT ensemble to maintain the volume of the system and control the temperature. Fig. 2.a illustrates a snapshot of the unhydroxylated silica surface.

Surface energies (γ_s) were calculated using:

$$\gamma_s = \frac{E_{US} - E_b}{A} \tag{5}$$

Eus is the energy of the unhydroxylated surface, E_b is the energy of the bulk system, and A is added surface area estimated as twice the cross sectional area. During surface formation two major defect types develop. The first are undercoordinated silicon atoms bonded to two or three oxygen atoms instead of four as in a typical SiO₄ tetrahedron. The second type of defect is a non-bridging oxygen (NBO) or oxygen atom bonded to one silicon atom. To create the hydroxylated surface, the unhydroxylated surfaces annealed at 1000K were used as the base structure. The surface coordination defects were terminated by either hydrogen atoms or hydroxide anions to form silanol (Si-OH) groups. Two-membered ring defects of two edge-sharing SiO₄ tetrahedra can also form. Reactions between water and strained two-membered ring sites result in the development of vicinal silanol groups due to siloxane bond breakage and opening of the two-membered ring ⁶¹. Here, the two-membered rings were removed by opening the ring and terminating the resulting three-coordinated silicon and NBO defects with hydroxide or hydrogen atoms respectively. A snapshot of a fully hydroxylated surface is included in Fig. 2b.

After hydroxylation a 300K annealing step was performed to allow for surface relaxation. The surface regions extended 7Å into the bulk, were heated to 300K, and after 200ps of simulation time with an NVT ensemble were quenched to 0K at a rate of 5K/ps. Surface energies were then calculated using:

198
$$\gamma_{s} = \frac{E_{HS} - (E_{b} - n * E_{H_{2}O})}{A} \tag{6}$$

 E_{HS} is the energy of the hydroxylated surface, E_b is the energy of the bulk silica, n is the number of water molecules consumed during the hydroxylation, and E_{H2O} is the energy of a water molecule. E_{H2O} account for the addition of oxygen and hydrogen atoms to the surface to terminate three-coordinated silicon and NBO defects 33 .

$$> Si + H_2O \rightarrow > Si - OH + H^+$$
 (7.a)

$$> Si - O^- + H^+ \rightarrow > Si - OH$$
 (7.b)

Water molecule energies were calculated by simulating an isolated water molecule in a 20Å simulation cell, a method which has been used in previous classical MD investigations of surface energies ^{27, 29}. A detailed discussion of the energies of bulk water and isolated water molecules between ClayFF and ReaxFF forcefields is included in the Results.

For comparison of Si-O bond strength, 192 atom β-cristobalite crystalline systems were generated and relaxed with the ClayFF and ReaxFF forcefields to remove the variability in structural features and intermediate range order of amorphous silica. The β-cristobalite simulation cell is then compressed or relaxed by scaling all the atomic positions changing the Si-O bond length in order to probe the bulk moduli and identify differences in how the forcefields simulate the Si-O bond energies. The total energy of the system divided by the number of Si-O bonds (~264 for a fully coordinated 192 atom β-cristobalite structure) forms an effective bond energy term. The complexity of the ReaxFF functional form limits the ability for a direct comparison of bond energies, since nearby atoms influence the energy of individual Si-O bonds. Therefore, the reported effective bond energies values discussed in the Results should not be mistaken for absolute differences in pairwise Si-O bond strength.

Pair distribution functions for the hydroxylated and unhydroxylated surfaces were compiled from 100,000 snapshots of the surface region to account for variations from thermal vibrations and the amorphous structure. A 2.25Å cut-off was used for interatomic distances and coordination numbers.

The connectivity was also calculated, and is the average number of bridging oxygen atoms bonded to a silicon atom, with 4.0 representing the structure of a perfectly coordinated silica glass composed entirely of four coordinated silicon (Q₄). The connectivity (C) is calculated from the distribution of Q_n species with n as the number of bridging oxygen (0-5) and C_{Qn} as the fraction of Q_n species 62 .

$$C = \sum_{n=0}^{5} n \cdot C_{Qn} \tag{8}$$

Variation in the surface structures has been accounted for by averaging results over three sets of surfaces formed with the addition of vacuum into the x-, y-, or z-dimensions. Error bars when reported are the standard deviation of these three systems.

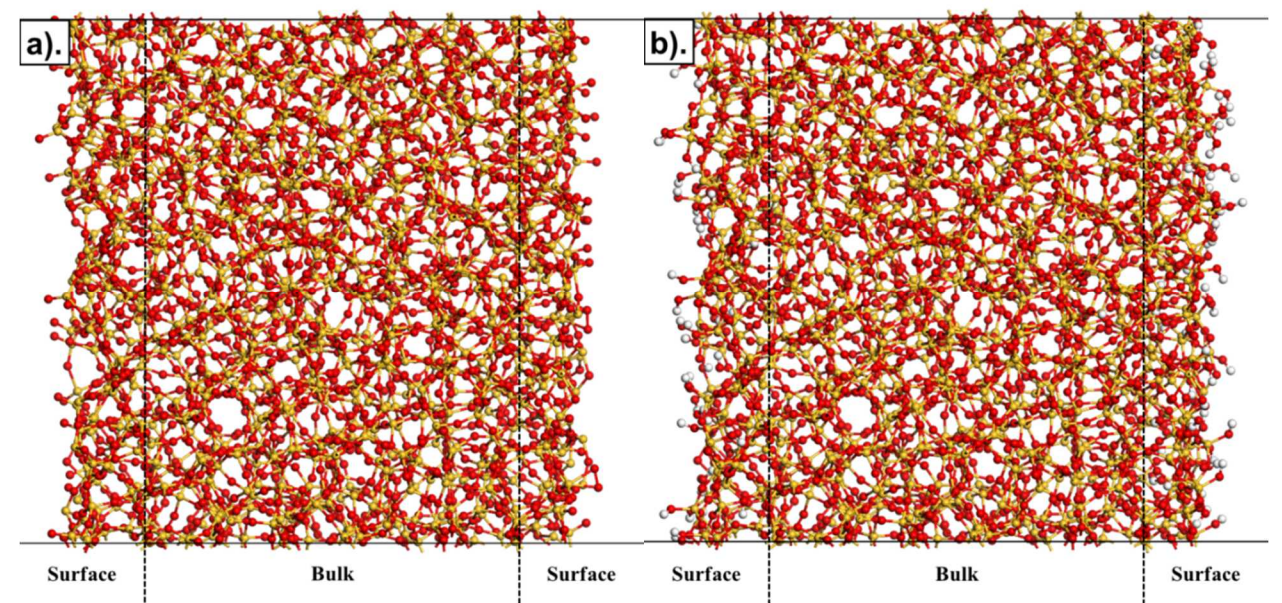


Figure 2: Snapshots of the (a) unhydroxylated silica and (b) hydroxylated silica surfaces, including the added hydroxide groups, simulated using the ReaxFF classical MD forcefield. Silicon (yellow), oxygen (red), hydrogen (white).

3. Results and Discussion

a. Silica Surface Structure and Annealing Temperature

Silica surfaces formed during fracture have different Si-O bond lengths and connectivity than bulk silica. Si-O pair distribution functions (PDFs) for bulk silica and three variations of the silica surface were calculated with both forcefields and are illustrated in Fig. 3. In all cases, the Si-O bond lengths are narrowly distributed around ~1.6Å, consistent with previous experimental and computational investigations ^{59, 63}. The ClayFF surfaces exhibit a pre-peak in the Si-O PDF at ~1.52Å for both unhydroxylated surfaces, with additional shorter Si-O bonds on the unrelaxed surface. More pronounced shortening of the Si-O bond occurs on the ReaxFF surfaces, with pre-peaks at ~1.37Å and ~1.41Å. The shortened Si-O bond lengths are NBO defects that disappear with hydroxylation. Previous classical MD investigations of silica surfaces found Si-NBO bond lengths are ~0.08Å shorter than the Si-O bond length, consistent with the ClayFF simulations presented here ⁶⁴. Only materials containing fully coordinated silicon were used in the parameterization of ClayFF, resulting in equilibrium Si-O bond lengths of ~1.6Å, with limited variation.

In comparison, ReaxFF simulations exhibit a much stronger contraction of the Si-NBO bonds than ClayFF surfaces. (Fig.3.b). The pre-peaks in the Si-O PDF data were identified as the

Si-NBO bond length by coordination number analysis, as well as by the lack of a pre-peak in the fully hydroxylated and bulk systems that do not contain NBO species. The shorter Si-NBO bond lengths are from the energy disassociation curve for the Si=O double bond in the H₂Si=O molecule used in the original parametrization of ReaxFF for Si/O systems ⁵³. As a result, ReaxFF simulates a contracted Si-NBO separation distance as ~1.4Å ⁵³. Other than the Si-NBO bond, no net change of the Si-O bond lengths occurs. Additional structural parameters, such as Si-Si, O-O, and O-H interatomic distances and O-Si-O and Si-O-H bond angles do not experience significant variation and are included in Table S1.



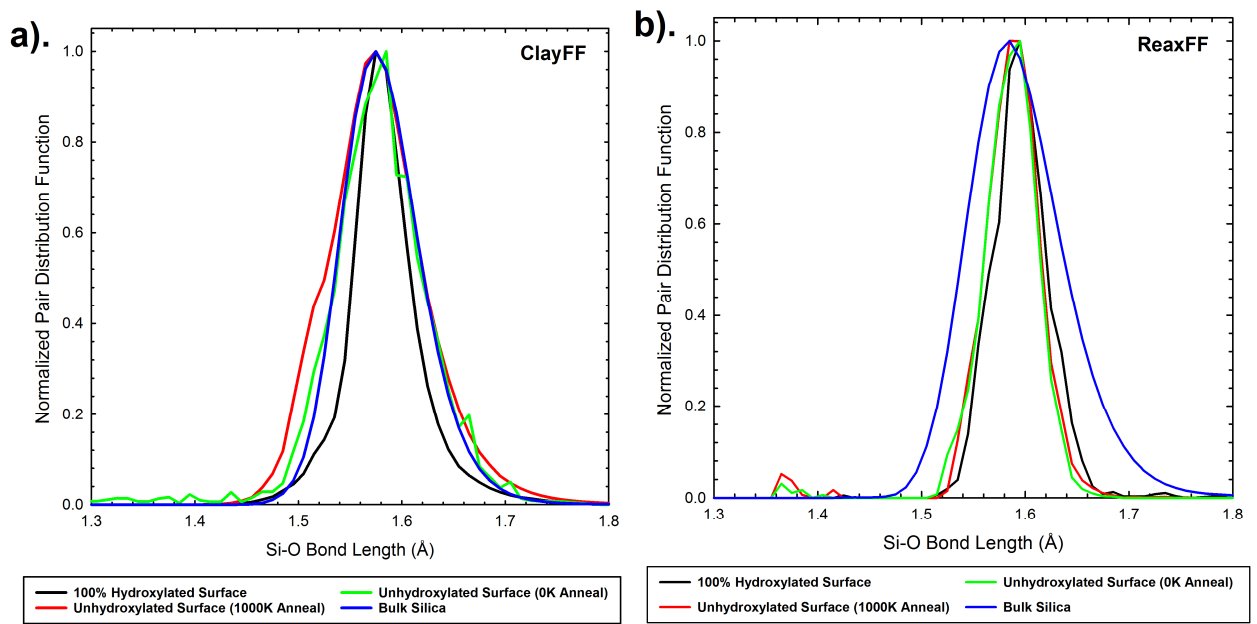


Figure 3: Si-O PDF for silica surfaces simulated with the (a) ClayFF and (b) ReaxFF classical MD forcefields.

Variation in the connectivity develops at the surface region, and Fig. 4 illustrates changes in surface connectivity as a function of annealing temperature. As the annealing temperature increases from 0K to 1000K, the surface connectivity asymptotically approaches ~3.71 for ReaxFF vs ~3.62 for ClayFF simulations. Further increases in annealing temperature are unlikely to alter the surface connectivity and even with high temperature annealing, the connectivity of the surface cannot be completely recovered ¹⁶. With the ReaxFF forcefield, the surface connectivity increases from 3.58 to 3.71, while with ClayFF, the connectivity only increases from 3.62 to 3.66 (Fig. 4). The surfaces simulated with the ReaxFF forcefield exhibited high

concentrations of both low Q_n (Q₃ and Q₂) and high (Q₅) species. Stable Q₅ concentrations of 4.4-4.6% developed regardless of annealing temperature. The Q₅ concentrations suggest that in ReaxFF calculations, the energy penalty of the Q₅ defect is less than for a NBO defect, resulting in an energetic preference for Q₅ species on the surface. The development of Q₅ species can be attributed to the original parametrization of ReaxFF, which includes the structure and properties of stishovite, a six-coordinated high pressure silicate polymorph 53 which may lead to the development of Q₅ species. Experimentally, magic angle spinning (MAS) nuclear magnetic resonance (NMR) has identified five-fold coordinated silicon in bulk glasses 65, indicating some stability of this defect structure. No clear experimental data exists on the relative stability of over- or under-coordination silicon on surface, other than that under coordinated silicon and oxygen defects are terminated within the first few nanoseconds of exposure to the environment ¹⁰. Under sufficiently high temperature conditions to remove all the hydroxyl groups, along with high vacuum conditions to limit further surface reactions, and time to allow for condensation of siloxane bonds the formation of stable over-bonded silicon concentrations may be possible. Due to the limited evidence for the development of Q₅ surface species from either experimental or DFT studies, the high Q₅ concentrations seen here are of some concern in the ability of ReaxFF to reproduce surface defect concentrations. Further investigations of competing defect termination energies would provide interesting insight into the relative stability of defects on silica surfaces.

In the ReaxFF simulations, decreases in Q_1 and Q_2 concentrations make up the majority of the recovered surface connectivity, with Q_2 species dropping from ~9% to ~4% between the 0K and 1000K anneal and Q_1 decreasing from ~0.9% to 0.1% (Table 1). Therefore, annealing results in removing the highest energy defects on the surface and increasing the Q_4 concentration.

The silica surfaces generated using the ClayFF forcefield are less defective, and contain higher concentrations of Q_4 species compared with the ReaxFF surfaces with no Q_5 or Q_1 species. As a result, decreases in the Q_2 and Q_3 concentrations with increases in annealing temperature are roughly linear and balanced by an increase in the Q_4 concentration on the surface. ClayFF parameters were selected to reproduce four-fold coordinated silicon in well-ordered crystals, such as quartz and kaolinite, as well as hydroxylated silica monomers $(Si(OH)_4)^{45}$. The development of three- or five-fold coordinated silicon atoms on dry silica

surfaces is partially determined by the forcefield parameters and may impact the surface energy due to the inclusion of higher energy defect species.

With the addition of silanols to the surface few changes in the Q_n distribution occur, with connectivity increasing by less than 0.04 for both ClayFF and ReaxFF simulations (Table S2). Without sufficient thermal energy to allow for removal of silanols and condensation of siloxane bonds, connectivity changes cannot occur during hydroxylation ⁶⁶.

In summary, the ClayFF forcefield exhibits stricter control over silicon coordination, limiting the development of defect species on the surface and altering the resultant surface energies.

Table 1: Q_n distribution of unhydroxylated silica surfaces after annealing.

	Q _n Species	1000K	700K	500K	300K	0K
ReaxFF Forcefield	Q_5	4.58±0.21	4.50±0.12	4.24±0.24	4.33±0.21	4.41±0.32
	Q_4	66.41±3.60	66.24±1.35	65.22±0.94	62.77±0.12	59.54±1.08
	Q ₃	24.94±2.53	24.77±2.24	25.74±2.12	26.63±1.93	26.29±2.34
	Q_2	3.99±0.86	4.41±0.86	4.41±1.07	5.68±1.41	8.91±0.95
	Q_1	0.08 ± 0.12	0.08 ± 0.12	0.25±0.41	0.59 ± 0.32	0.85±0.12
ClayFF Forcefield	Q ₄	70.21±1.43	69.63±1.79	68.89±2.05	67.41±1.45	67.00±0.99
	Q_3	26.91±1.94	27.65±2.13	27.98±2.22	29.30±1.42	28.64±0.88
	Q_2	2.88±0.62	2.72±0.35	3.13±0.51	3.29 ± 0.23	4.20±0.20

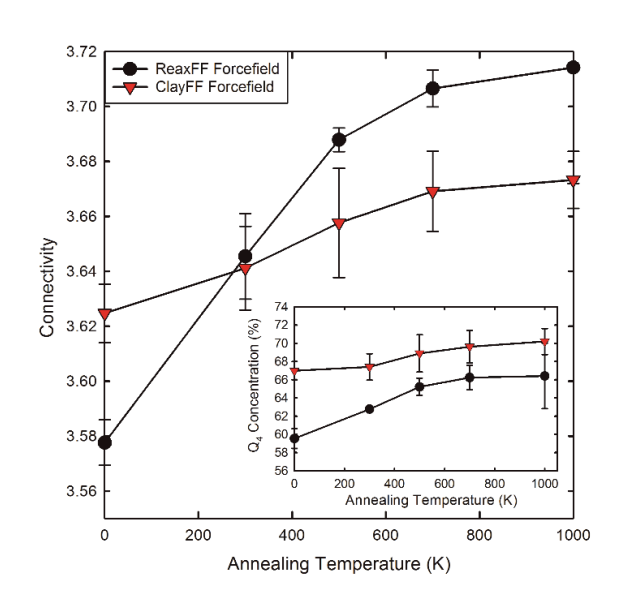


Figure 4: Connectivity of unhydroxylated silica surfaces after annealing and the concentration of Q₄ species (inset)

b. Surface Energies of Unhydroxylated Silica Surfaces

324

325

326

327

328

329

330

331

332

333

334

335

336

337

338

339

340

341

342

343

344

345

346

347

348

349

350

351

352

353

354

Calculated differences in the surface energies of unhydroxylated silica arise from the surface structure and the description of siloxane bond and defect energies in the forcefields. Surface energies from the ClayFF simulations are considerably higher than from the ReaxFF simulations (Fig. 5), and exhibit a smaller decrease after high temperature annealing. The relative difference in the surface energies may be a result of the Si-O description, with the ClayFF forcefield assigning a strong energy penalty to broken Si-O bonds. Effective Si-O bond energies in Fig. 6 demonstrate that both forcefields result in similar effective bond energies during expansion of the β-cristobalite unit cell. During compression, the behavior deviates between the two forcefields, with the ReaxFF forcefield exhibiting effective bond energies nearly 80 kJ/mol lower than the ClayFF simulations for volume compressions between 0 and -20%. Therefore, compression of Si-O bonds results in smaller changes in effective bond energy for the ReaxFF forcefield. Previously noted contraction in the Si-O bond distances in the surface region will be more energetically unfavorable with the ClayFF forcefield, resulting in higher surface energies. The lower effective bond energies calculated with ReaxFF may arise from the validation of the original Si/O parametrization of ReaxFF with equations of state for silica polymorphs αcristobalite, coesite, and stishovite 53. Since the Si/O parametrizations of ReaxFF are fit to a much wider range of silicate structures than ClayFF, which has been rigorously parameterized for aluminosilicates, changes in the Si-O bond length does not result in the same energy penalty as in the ClayFF systems.

While the treatment of Si-O bonds may account for the absolute differences in the surface energies, decreases in surface energy during high temperature relaxation (Fig.5) are instead connected with the surface structure. The surface energy calculated using ClayFF forcefield decreases from 5.13 J/m² to 4.93 J/m² after annealing at 1000K. As the annealing temperature increases so does the surface connectivity, which decreases both defect concentration and the surface energy. This relationship is roughly linear (Fig.5) which indicates that the ClayFF surfaces exhibit a decrease in surface energies with increases in coordination.

On the silica surfaces simulated using the ReaxFF forcefield, surface energies decrease from 2 J/m² to 1.2 J/m² with increasing annealing temperature, 4x the change in surface energies on the ClayFF simulated surfaces. This difference (Fig. 5) is also seen in the linear fit of the data with ClayFF simulations having a slope of -4.39 and ReaxFF having a slope of -5.39 for

connectivity versus surface energy. Therefore, the ReaxFF forcefield is more sensitive to the connectivity of the surface than the ClayFF forcefield.

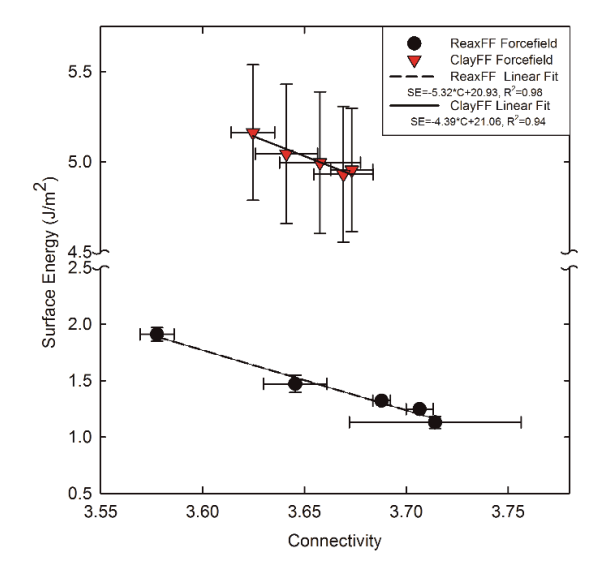


Figure 5: Surface energies of unhydroxylated surfaces with connectivity. The linear fit of the surface energy (SE) with the connectivity (C) is included.

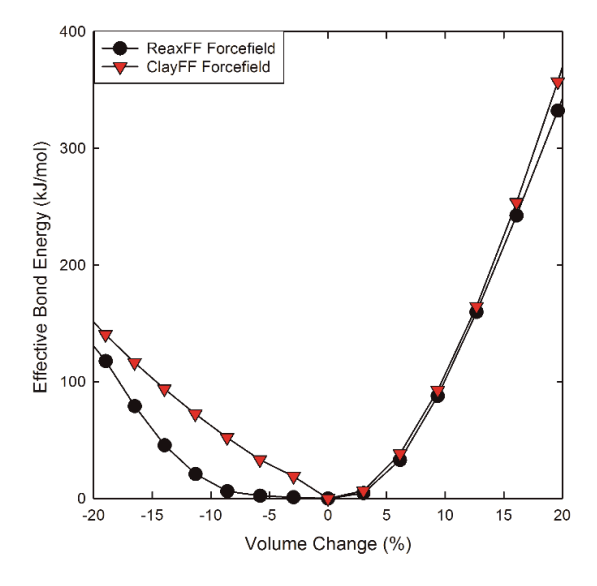


Figure 6: Effective bond energy with volume change for β -cristobalite.

c. Surface Energies of Hydroxylated Silica Surfaces

Reported silica surface energies vary with experimental method, silica microstructure and composition, as well as the silica polymorphs (Fig. 1). Surface energies are often reported for fully hydroxylated systems due to the instability of partially hydroxylated surfaces ⁴¹. Under

atmospheric conditions, hydroxylated silica surfaces have silanol concentrations between 4-5/nm² which volatize under high vacuum ⁶⁷. Here, fully hydroxylated surfaces created from 1000K annealed silica surfaces, have silanol densities of 4.33±0.26/nm² for the ClayFF simulations and 4.04±0.26 #/nm² for the ReaxFF simulations (Table 2). Three types of silanol groups can form on silica surfaces. These include geminal silanols (two hydroxyl groups bonded to the same silicon), vicinal silanols (two hydroxyl groups bonded to adjacent silicons), and isolated silanol groups. Silica surfaces simulated with ReaxFF have higher concentrations of geminal silanols than those simulated with ClayFF. The higher geminal silanol concentration is balanced by lower concentrations of isolated silanols, indicating that these surfaces contain higher concentrations of two-membered rings, which are opened to form hydroxyl groups. Under high temperature treatment both vicinal and geminal silanols condense to form siloxane bonds, and the higher concentration of isolated silanol groups on the ClayFF surface provides evidence for why the Q_n distribution is more stable. Additionally, the distribution of silanols loosely follows the Zhuravlev experimental analysis, which identifies high vicinal silanol concentrations (1.65/nm²), intermediate isolated silanol concentrations (1.40/nm²), and low geminal silanol concentrations (0.50/nm²) on silica surfaces after a 600K pretreatment ⁶⁷. At room temperatures the concentration of vicinal silanol groups on experimental silica surfaces increases sharply to 2.80/nm², and that of isolated silanols decreases to 1.20/nm² ⁶⁷. Due to the high temperature annealing used here, which results in condensation of adjacent coordination defects as seen in the On distribution; both forcefields are consistent with the data for silica surfaces after an annealing pre-treatment.

367

368

369

370

371

372

373

374

375

376

377

378

379

380

381

382

383

384

385

386

387

388

389

390

391

392

393

394

395

396

397

Using ClayFF, the surface energy of an unhydroxylated surface is 4.96±0.34 J/m² and decreases to 4.41±0.25 J/m² for a fully hydroxylated surface (Fig. 7). The surface energies for ReaxFF surfaces are lower, at 1.13 J/m² for unhydroxylated surfaces after 1000K annealing, and dropping to ~0.15 J/m² after complete hydroxylation. The surface energies reported from ClayFF simulations match well with experimental data from DCB tests on silica in nitrogen atmospheres by Wiederhorn ²³. Therefore, the ClayFF results are more consistent with experimental data for fracture surfaces. After a 1000K annealing step and full hydroxylation it is expected that the surface would be at a low energy equilibrium state. Surface energies for equilibrium surfaces are measured as ~0.35 J/m², which is most consistent with the ReaxFF data³⁹. Therefore, for the simulation of fracture studies it appears that the higher surface energies from ClayFF simulations

are more accurate, while ReaxFF simulations match better with available data from equilibrium surfaces.

Surface energies decrease with increasing silanol concentration regardless of which classical MD forcefield is used. Experimental data also identifies decreases in surface energies with hydroxylation, though the relationship is inferred through changes in the water-silica surface. For example, a reduction in surface energy of 0.1-0.2 J/m² with hydroxylation has been inferred by Rückriem et al. through the use of inverse gas chromatography in porous systems ⁶⁸. Mahadik et al. also noted a loosely linear relationship with an increase in the water-silica contact angle of 130° from SEM images and a decrease in the surface energy of ~0.11 J/m² on silica aerogels ⁶⁹. Over the entire hydroxylation range surface energies from ClayFF simulations decrease by ~0.5 J/m², which is more consistent with experimental decreases in the surface energy.

The energetics of the water molecule impacts how the forcefield describes surface energies of hydroxylated silica, since the strength of the added O-H bond and removal of defects lowers the surface energy. The self-energy of a water molecule is used to account for added oxygen and hydrogen atoms to the system, since water disassociates into hydrogen and hydroxide groups on the surface ²⁷. Several previous classical MD investigations of surface energies of minerals including quartz (SiO₂) ²⁷, hematite (Fe₂O₃) ⁷⁰, fluroapatite (Ca₅(PO₄)₃F) ⁷¹, and dolomite (CaMg(CO₃)₂) ⁷² have used the self-energy of water molecules to account for the addition of hydroxide bonds on the surface. Water energies from ReaxFF and ClayFF forcefields are in Table 3, including the self-energy of a water molecule and the average energy of a water molecule in a bulk water simulation cell (20Åx20Åx20Å) containing 343 water molecules. The self-energy of the SPC water molecule arises from either the harmonic bond stretching and angle terms or from O-O interactions between adjacent water molecules, with the other parameters set to zero ⁴⁵ ⁷³ resulting in a self-energy of -0.10±0.002 kJ/mol ⁷³. The average molecular energy of bulk water is -44.51±0.34 kJ/mol and is consistent with previous reported values for the energy of the SPC water molecules of -45.3 kJ/mol ⁷³.

In contrast, the ReaxFF forcefield contains a strong O-H bond in the water molecule and the self-energy of a water molecule is -1010.45±4.24 kJ/mol compared to -1052.54±0.36 kJ/mol in bulk water (Table 3). The ReaxFF forcefield is parametrized to the cohesive energy of water, or the difference in average molecular energy of bulk water and the self-energy of a water

molecule ⁷⁴. De Leeuw and Parker implemented a shell-model water potential with an energy of vaporization of ~43.0 kJ/mol and a self-energy of -878.0 kJ/mol for calculating surface energies of hydroxylated α-quartz ⁷⁵. Self-energies of water between -670 kJ/mol and -710 kJ/mol and cohesive energies of -42 kJ/mol to -50.2 kJ/mol have also been reported for classical MD forcefields of water-silica systems by Mahadevan and Garofalini 74. Wide variation in water selfenergy occurs since most water models, including SPC and ReaxFF water, are parametrized to match the experimental cohesive energy of water, ~44kJ/mol ⁷⁶. The self-energy of water is most critical when the silica surface is hydroxylated, but when bulk water is present the intermolecular forces allow for hydrogen bonding and further surface relaxation. To identify the effect of bulk water on surface energy, bulk water was added to the vacuum space in the fully hydroxylated system. First the hydroxylated silica was frozen and the system was relaxed for 100ps at 0.1K to calculate the added energy from hydrogen bonding and binding between the water and the surface. Then, the silica surface and the water were relaxed simultaneously for 100ps at 0.1K to calculate the change in the surface structure in the presence of bulk water. The resulting surface energy calculated with ClayFF decreases by 0.56±0.49 J/m², indicating that a significant amount of surface relaxation occurs. In comparison, the ReaxFF surface energy decreases by only 0.09±0.01 J/m². This minor change in energy for ReaxFF may be because reactivity cannot be turned off in ReaxFF; therefore, interactions between water and silica occur even when the surface is frozen.

429

430

431

432

433

434

435

436

437

438

439

440

441

442

443

444

445

446

447

448

449

450

451

452

453

454

455

The energetics of the selected water model affects how hydroxylation alters the surface energies, and therefore must be chosen with care to match with experimental values. In this case the low self-energy of SPC water suggests that its application for fracture surfaces would be an advantage, since the resultant surface energies match best with reported experimental fracture surface energies. Alternatively, the high self-energy of water in the ReaxFF potential results in a lower surface energies of $\sim 0.2 \text{ J/m}^2$ for a fully hydroxylated and relaxed surface, consistent with the equilibrium surface energies of $\sim 0.35 \text{ J/m}^2$.

Table 2: Silanol concentration on fully and partially hydroxylated surfaces simulated using the ClayFF or ReaxFF classical MD forcefield.

Clay11 of Reax11 classical MD foreclicity.								
	Total		Geminal		Vicinal		Isolated	
Hydroxyl Coverage	ClayFF	ReaxFF	ClayFF	ReaxFF	ClayFF	ReaxFF	ClayFF	ReaxFF
100%	4.30	4.04	0.91	1.29	1.89	1.65	1.50	1.10
	± 0.24	±0.26	±0.10	± 0.17	± 0.12	±0.09	±0.21	± 0.05
80%	3.50	3.33	0.62	0.97	1.29	1.21	1.58	1.15
	± 0.23	±0.22	±0.10	±0.20	± 0.03	±0.16	±0.24	±0.24
60%	2.65	2.49	0.24	0.47	0.68	0.75	1.72	1.25
	± 0.21	±0.17	± 0.00	±0.17	±0.21	±0.09	±0.21	±0.20
40%	1.77	1.67	0.00	0.18	0.32	0.38	1.48	1.10
	± 0.13	±0.10	± 0.00	±0.13	± 0.09	± 0.05	±0.09	±0.20
20%	0.88	0.79	0.00	0.11	0.07	0.12	0.82	0.56
	± 0.07	± 0.00	± 0.00	± 0.07	± 0.09	±0.12	±0.15	±0.15

Table 3: Self-energy and average molecular energy of water in the ClayFF and ReaxFF forcefields.

Energy (kJ/mol)	ClayFF Forcefield	ReaxFF Forcefield	
Self-Energy of Water Molecule	-0.099±0.002	-1010.45±4.24	
Bulk Water Energy (per Molecule)	-44.51±0.34	-1052.54±0.36	
Cohesive Energy	-44.41	-42.09	

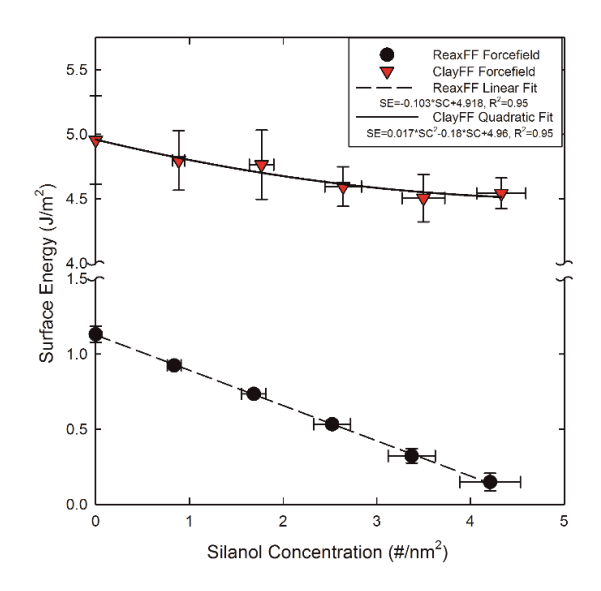


Figure 7: Surface energies with hydroxylation content for silica surfaces simulated using ClayFF and ReaxFF classical MD forcefields. The linear fit (ReaxFF) or quadratic fix (ClayFF) of the surface energy (SE) with the connectivity (C) for the two forcefields is included.

4. Summary and Conclusions

467

468

469

470

471

472

473

474

475

476

477

478

479

480

481

482

483

484

485

486

487

488

489

490

491

492

493

494

495

496

497

Changing surface energies of silica caused by annealing and hydroxylation influence crack propagation during brittle fracture and impact the response of silica to environmental conditions. Hence, accurate surface energies play a key role in the simulation of fracture. In this work, the role of classical molecular dynamics (MD) forcefields on the structure and energies of silica surfaces was investigated using two different forcefields capable of modeling the interaction of silica glass with ambient water: ClayFF forcefield, a two-bodied Lennard-Jones potential combined with a SPC water model 45 and ReaxFF forcefield, a reactive bond order based forcefield ⁵⁷. Annealing silica surfaces resulted in an increase in the surface connectivity and a decrease in the surface energies due to the reformation of siloxane bonds. ReaxFF simulated dry surfaces had surface energies between 1.2-2.0 J/m² and developed concentrations of fivecoordinated silicon atoms, increasing the surface connectivity. In contrast, the ClayFF surfaces exhibited much higher surface energies, 5.0-5.2 J/m², which are consistent with reported experimental fracture surface energies of ~4.5 J/m² ²³. In neither case did fracto-emission of either Si or O atoms occur. This effect has primarily been observed in alkali glasses⁷⁷⁻⁷⁹. Hydroxylation of the annealed surfaces resulted in decreases in surface energies associated with silica surface equilibration in the presence water. ClayFF surface energies decreased by only ~0.5 J/m² to 4.5 J/m² while ReaxFF surfaces had a final equilibrium surface energy of 0.2 J/m². consistent with experimentally measured equilibrium surface energies of ~0.35 J/m^{2 39}. The selfenergy of the water molecules in the forcefields impacted the hydroxylated surface energies due to the inclusion of O-H bonds on the surface. Water molecules in the ReaxFF forcefield have a more energetic O-H bond resulting in surface energies decreasing by 1.0 J/m² compared with 0.5 J/m² in the ClayFF forcefield.

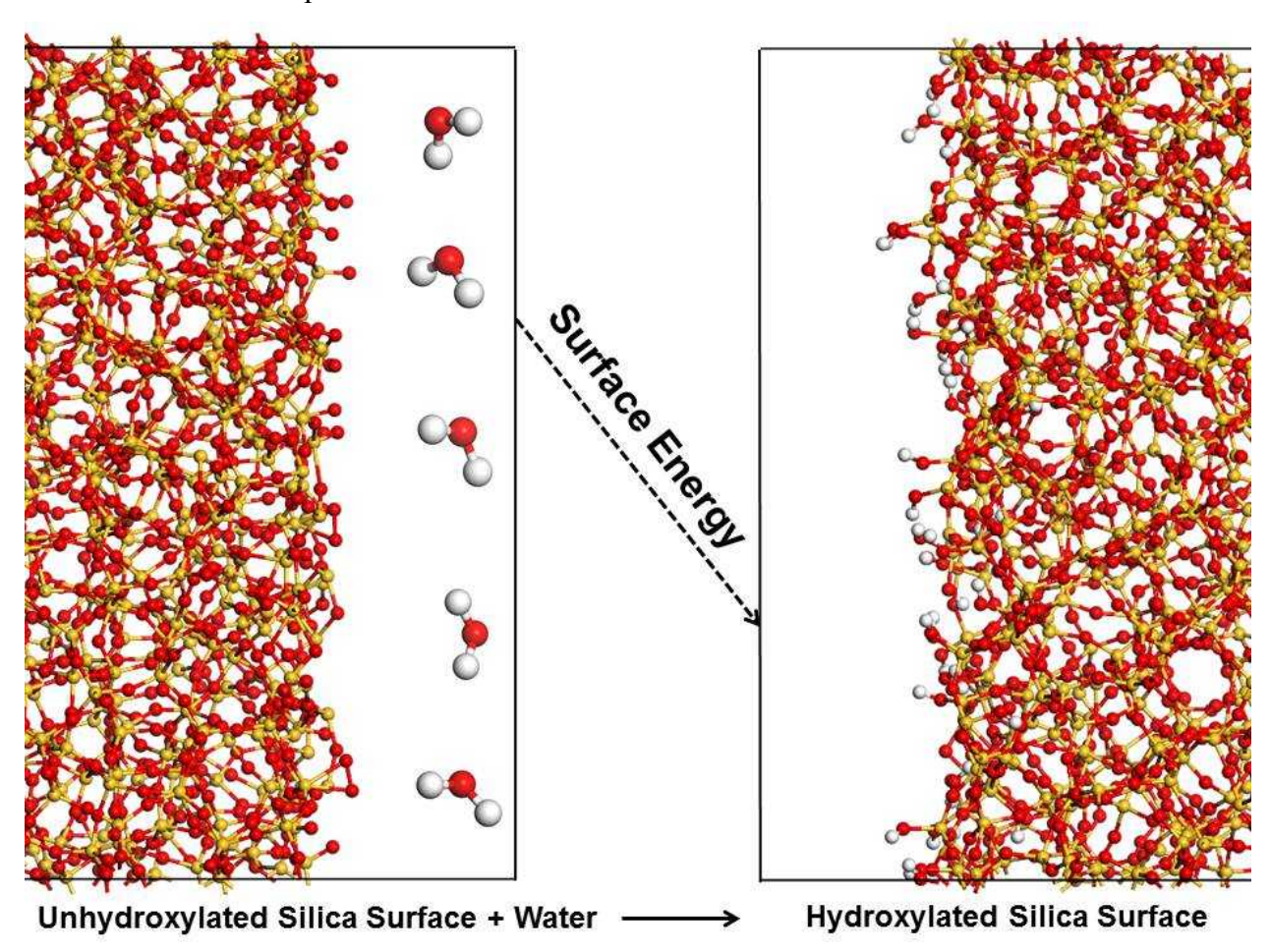
Ultimately, neither of the two forcefields explored in this work was capable of accurately replicating both the experimentally reported high-energy unhydroxylated fracture surface energies and the annealed and hydroxylated equilibrium surface energies. Calculated surface energies with the ClayFF forcefield are more consistent with experimental fracture surface energy values, even after simulated annealing and hydroxylation which approximate the effect of surface relaxation and development of a low-energy equilibrium surface. The ReaxFF forcefield under-estimated fracture surface energies and exhibited more significant structural relaxation and decreases in surface energy with hydroxylation, resulting in equilibrium surface energies which

are consistent with experiment. Therefore, future studies of silica which rely on the energetics of added surface area, such as silica fracture, should consider the environment and level of surface relaxation, and select a classical or reactive forcefield which reproduces the appropriate conditions. Further investigation of silica-water interfaces would benefit from the development of forcefields parametrized to surface structure and energetics to ensure accurate models across a variety of different surface conditions.

Acknowledgement: This work was fully supported by the Laboratory Directed Research and Development (LDRD) program of Sandia National Laboratories. Sandia is a multi-mission laboratory operated by Sandia Corporation, a Lockheed Martin company, for the U.S. Department of Energy under Contract DE-AC04-94AL85000

Supporting Information Available: The peak and full-width-at-half-max values for the Si-Si, O-O, and O-H pair distribution functions (PDF) and O-Si-O and Si-O-H bond angle distributions (BAD) for silica surfaces are included in supporting information (Table S1). The changing Q_n speciation as a function of the hydroxylation content is also included (Table S2). This material is available free of charge via the internet at http://pubs.acs.org.

Table of Contents Graphic



- 520 References
- 521 (1. Power, W. L.; Tullis, T. E., The relationship between slickenside surfaces in fine-grained quartz
- and the seismic cycle. *Journal of Structural Geology* **1989,** *11* (7), 879-893.
- 523 2. Parks, G. A., Surface and interfacial free energies of quartz. *Journal of Geophysical Research:*
- 524 *Solid Earth* **1984,** *89* (B6), 3997-4008.
- 525 3. Schlegel, M. L.; Nagy, K. L.; Fenter, P.; Sturchio, N. C., Structures of quartz (100)-and (101)-water
- 526 interfaces determined by x-ray reflectivity and atomic force microscopy of natural growth surfaces.
- 527 *Geochimica et Cosmochimica acta* **2002,** *66* (17), 3037-3054.
- 528 4. Tullis, J.; Yund, R. A., Hydrolytic weakening of quartz aggregates: The effects of water and
- pressure on recovery. *Geophysical Research Letters* **1989**, *16* (11), 1343-1346.
- 530 5. Giordano, L.; Sushko, P.; Pacchioni, G.; Shluger, A., Optical and EPR properties of point defects at
- a crystalline silica surface: Ab initio embedded-cluster calculations. *Physical Review B* **2007**, *75* (2),
- 532 024109.
- 6. Grosse, A.; Grewe, M.; Fouckhardt, H., Deep wet etching of fused silica glass for hollow capillary
- optical leaky waveguides in microfluidic devices. Journal of micromechanics and microengineering 2001,
- 535 11 (3), 257.
- 536 7. Wurzbacher, J. A.; Gebald, C.; Steinfeld, A., Separation of CO2 from air by temperature-vacuum
- 537 swing adsorption using diamine-functionalized silica gel. Energy & Environmental Science 2011, 4 (9),
- 538 3584-3592.
- 8. Adeyemo, A.; Kumar, R.; Linga, P.; Ripmeester, J.; Englezos, P., Capture of carbon dioxide from
- flue or fuel gas mixtures by clathrate crystallization in a silica gel column. *International Journal of*
- 541 Greenhouse Gas Control **2010**, 4 (3), 478-485.
- 542 9. Najafi, M.; Yousefi, Y.; Rafati, A., Synthesis, characterization and adsorption studies of several
- heavy metal ions on amino-functionalized silica nano hollow sphere and silica gel. Separation and
- 544 *Purification Technology* **2012,** *85*, 193-205.
- 545 10. D'Souza, A. S.; Pantano, C. G., Hydroxylation and dehydroxylation behavior of silica glass fracture
- surfaces. *Journal of the American Ceramic Society* **2002,** *85* (6), 1499-1504.
- 547 11. Leed, E. A.; Pantano, C. G., Computer modeling of water adsorption on silica and silicate glass
- fracture surfaces. *Journal of Non-Crystalline Solids* **2003**, *325* (1), 48-60.
- 549 12. Mueller, M.; Pejchal, V.; Žagar, G.; Singh, A.; Cantoni, M.; Mortensen, A., Fracture toughness
- 550 testing of nanocrystalline alumina and fused quartz using chevron-notched microbeams. Acta Materialia
- **2015**, *86*, 385-395.
- 552 13. Kimura, Y.; Yagasaki, T.; Kunio, T., On the delayed fracture characteristics of Vickers indented
- glass in deionized water. Engineering fracture mechanics **1984**, 19 (6), 1025-1033.
- 14. Haranoh, T.; Ishikawa, H.; Shinkai, N.; Mizuhashi, M., Crack evolution in Vickers indentation for
- soda-lime-silica glass. *Journal of Materials Science* **1982,** *17* (5), 1493-1500.
- 556 15. Weichert, R.; Schönert, K., Heat generation at the tip of a moving crack. Journal of the
- 557 *Mechanics and Physics of Solids* **1978,** *26* (3), 151-161.
- 558 16. Fineberg, J.; Marder, M., Instability in dynamic fracture. *Physics Reports* **1999**, *313* (1), 1-108.
- 559 17. Fuller, K.; Fox, P.; Field, J. In *The temperature rise at the tip of fast-moving cracks in glassy*
- 560 polymers, Proceedings of the Royal Society of London A: Mathematical, Physical and Engineering
- 561 Sciences, The Royal Society: 1975; pp 537-557.
- 562 18. Newby, J. J.; Legg, M. A.; Rogers, B.; Wirth, M. J., Annealing of silica to reduce the concentration
- of isolated silanols and peak tailing in reverse phase liquid chromatography. *Journal of Chromatography*
- 564 *A* **2011**, *1218* (31), 5131-5135.
- 565 19. Maugis, D., Subcritical crack growth, surface energy, fracture toughness, stick-slip and
- 566 embrittlement. *Journal of materials Science* **1985,** *20* (9), 3041-3073.
- 567 20. Orowan, E., The fatigue of glass under stress. *Nature* **1944**, *154* (3906), 341-343.

- 568 21. Lawn, B.; Wilshaw, R., Indentation fracture: principles and applications. *Journal of materials*
- 569 science **1975**, 10 (6), 1049-1081.
- 570 22. Ciccotti, M., Stress-corrosion mechanisms in silicate glasses. *Journal of physics D: Applied physics*
- **2009,** *42* (21), 214006.
- 572 23. Wiederhorn, S. M., Fracture surface energy of glass. *Journal of the American Ceramic Society*
- 573 **1969,** *52* (2), 99-105.
- 574 24. Wiederhorn, S.; Shorb, A.; Moses, R., Critical Analysis of the Theory of the Double Cantilever
- 575 Method of Measuring Fracture-Surface Energies. *Journal of Applied Physics* **1968**, *39* (3), 1569-1572.
- 576 25. Nakayama, J., Direct measurement of fracture energies of brittle heterogeneous materials.
- 577 *Journal of the American Ceramic Society* **1965,** *48* (11), 583-587.
- 578 26. Murashov, V. V., Reconstruction of pristine and hydrolyzed quartz surfaces. The Journal of
- 579 *Physical Chemistry B* **2005**, *109* (9), 4144-4151.
- 580 27. de Leeuw, N. H.; Higgins, F. M.; Parker, S. C., Modeling the surface structure and stability of α -
- 581 quartz. The Journal of Physical Chemistry B **1999**, 103 (8), 1270-1277.
- 582 28. Goumans, T.; Wander, A.; Brown, W. A.; Catlow, C. R. A., Structure and stability of the (001) α-
- quartz surface. *Physical Chemistry Chemical Physics* **2007**, *9* (17), 2146-2152.
- 584 29. Bandura, A. V.; Kubicki, J. D.; Sofo, J. O., Periodic density functional theory study of water
- adsorption on the α-Quartz (101) surface. The Journal of Physical Chemistry C 2011, 115 (13), 5756-
- 586 5766.
- 587 30. Murashov, V. V.; Demchuk, E., Surface sites and unrelaxed surface energies of tetrahedral silica
- polymorphs and silicate. Surface science **2005**, 595 (1), 6-19.
- 589 31. Grillo, M. E.; Coll, D. S.; Rodríguez, J., Effect of the environment on the hydroxyl density of α-
- 590 quartz (111). Chemical Physics Letters **2012**, 522, 46-50.
- 591 32. Goniakowski, J.; Noguera, C., Electronic structure of clean insulating oxide surfaces I. A
- 592 numerical approach. *Surface science* **1994,** *319* (1), 68-80.
- 593 33. Shchipalov, Y. K., Surface energy of crystalline and vitreous silica. *Glass and ceramics* **2000**, *57*
- 594 (11-12), 374-377.
- 34. Rignanese, G.-M.; De Vita, A.; Charlier, J.-C.; Gonze, X.; Car, R., First-principles molecular-
- dynamics study of the $(0001) \alpha$ q u a r t z surface. *Physical Review B* **2000**, *61* (19), 13250.
- 597 35. Chagarov, E.; Demkov, A. A.; Adams, J. B., Ab initio calculations of surface phase diagrams of
- 598 silica polymorphs. *Physical Review B* **2005,** *71* (7), 075417.
- 36. Jurewicz, S. R.; Watson, E. B., Distribution of partial melt in a felsic system: the importance of
- surface energy. Contributions to Mineralogy and Petrology **1984**, 85 (1), 25-29.
- 601 37. Wiederhorn, S. M.; Johnson, H., Effect of pressure on the fracture of glass. *Journal of Applied*
- 602 *Physics* **1971,** *42* (2), 681-684.
- 603 38. Vigil, G.; Xu, Z.; Steinberg, S.; Israelachvili, J., Interactions of silica surfaces. Journal of Colloid and
- 604 interface science **1994**, 165 (2), 367-385.
- 605 39. Varshneya, A. K., Fundamentals of inorganic glasses. Elsevier: 2013.
- 606 40. Hammond, M.; Ravitz, S., Influence of environment on brittle fracture of silica. Journal of the
- 607 American Ceramic Society **1963**, 46 (7), 329-332.
- 608 41. D'Souza, A. S.; Pantano, C. G.; Kallury, K. M., Determination of the surface silanol concentration
- of amorphous silica surfaces using static secondary ion mass spectroscopy. Journal of Vacuum Science &
- 610 Technology A **1997**, 15 (3), 526-531.
- 611 42. Tsuneyuki, S.; Tsukada, M.; Aoki, H.; Matsui, Y., First-principles interatomic potential of silica
- applied to molecular dynamics. *Physical Review Letters* **1988**, *61* (7), 869.
- 613 43. Van Beest, B.; Kramer, G. J.; Van Santen, R., Force fields for silicas and aluminophosphates based
- on ab initio calculations. *Physical Review Letters* **1990**, *64* (16), 1955.

- 615 44. Du, Z.; de Leeuw, N. H., A combined density functional theory and interatomic potential-based
- simulation study of the hydration of nano-particulate silicate surfaces. Surface Science 2004, 554 (2),
- 617 193-210.
- 618 45. Cygan, R. T.; Liang, J.-J.; Kalinichev, A. G., Molecular models of hydroxide, oxyhydroxide, and clay
- 619 phases and the development of a general force field. The Journal of Physical Chemistry B 2004, 108 (4),
- 620 1255-1266.
- 46. Ho, T. A.; Argyris, D.; Papavassiliou, D. V.; Striolo, A.; Lee, L. L.; Cole, D. R., Interfacial water on
- 622 crystalline silica: a comparative molecular dynamics simulation study. *Molecular Simulation* **2011,** *37*
- 623 (03), 172-195.
- 624 47. Bourg, I. C.; Steefel, C. I., Molecular dynamics simulations of water structure and diffusion in
- 625 silica nanopores. *The Journal of Physical Chemistry C* **2012**, *116* (21), 11556-11564.
- 626 48. Kroutil, O.; Chval, Z.; Skelton, A.; Předota, M., Computer Simulations of Quartz (101)–Water
- Interface over a Range of pH Values. The Journal of Physical Chemistry C 2015, 119 (17), 9274-9286.
- 628 49. Skelton, A.; Wesolowski, D. J.; Cummings, P. T., Investigating the Quartz (10T0)/Water Interface
- Using Classical and Ab Initio Molecular Dynamics. *Langmuir* **2011**, *27* (14), 8700-8709.
- 630 50. Skelton, A.; Fenter, P.; Kubicki, J. D.; Wesolowski, D. J.; Cummings, P. T., Simulations of the
- quartz (1011)/water interface: a comparison of classical force fields, ab initio molecular dynamics, and X-
- ray reflectivity experiments. *The Journal of Physical Chemistry C* **2011,** *115* (5), 2076-2088.
- 633 51. Wander, M. C.; Clark, A. E., Structural and dielectric properties of quartz- water interfaces. The
- 634 *Journal of Physical Chemistry C* **2008,** *112* (50), 19986-19994.
- 635 52. Aktulga, H. M.; Fogarty, J. C.; Pandit, S. A.; Grama, A. Y., Parallel reactive molecular dynamics:
- Numerical methods and algorithmic techniques. *Parallel Computing* **2012**, *38* (4), 245-259.
- 53. Van Duin, A. C.; Strachan, A.; Stewman, S.; Zhang, Q.; Xu, X.; Goddard, W. A., ReaxFFSiO reactive
- force field for silicon and silicon oxide systems. *The Journal of Physical Chemistry A* **2003,** *107* (19), 3803-3811.
- 54. Zheng, M.; Li, X.; Guo, L., Algorithms of GPU-enabled reactive force field (ReaxFF) molecular
- dynamics. *Journal of Molecular Graphics and Modelling* **2013,** *41*, 1-11.
- 642 55. Fogarty, J. C.; Aktulga, H. M.; Grama, A. Y.; Van Duin, A. C.; Pandit, S. A., A reactive molecular
- dynamics simulation of the silica-water interface. The Journal of chemical physics 2010, 132 (17),
- 644 174704.
- 645 56. Manzano, H.; Moeini, S.; Marinelli, F.; Van Duin, A. C.; Ulm, F.-J.; Pellenq, R. J.-M., Confined
- water dissociation in microporous defective silicates: mechanism, dipole distribution, and impact on
- substrate properties. *Journal of the American Chemical Society* **2012**, *134* (4), 2208-2215.
- 648 57. Yeon, J.; van Duin, A. C., ReaxFF Molecular Dynamics Simulations of Hydroxylation Kinetics for
- 649 Amorphous and Nano-Silica Structure, and Its Relations with Atomic Strain Energy. The Journal of
- 650 *Physical Chemistry C* **2015**, *120* (1), 305-317.
- 651 58. Rimsza, J. M.; Yeon, J.; van Duin, A. C.; Du, J., Water Interactions With Nanoporous Silica:
- 652 Comparison of ReaxFF and Ab Initio Based Molecular Dynamics Simulations. The Journal of Physical
- 653 Chemistry C **2016**.
- 654 59. Mozzi, R.; Warren, B., The structure of vitreous silica. *Journal of Applied Crystallography* **1969**, 2
- 655 (4), 164-172.
- 656 60. Plimpton, S., Fast parallel algorithms for short-range molecular dynamics. *Journal of*
- 657 *computational physics* **1995,** *117* (1), 1-19.
- 658 61. Rimsza, J.; Du, J., Ab initio Molecular Dynamics Simulations of the Hydroxylation of Nanoporous
- 659 Silica. *Journal of the American Ceramic Society* **2015**, *98* (12), 3748-3757.
- 660 62. Du, J.; Xiang, Y., Effect of strontium substitution on the structure, ionic diffusion and dynamic
- properties of 45S5 Bioactive glasses. *Journal of Non-Crystalline Solids* **2012**, *358* (8), 1059-1071.

- 662 63. Rimsza, J.; Van Duin, A. C.; Du, J., Comparison of ReaxFF and ab initio molecular dynamics for
- water-nanoporous silica interactions. **2016**.
- 664 64. Garofalini, S., A molecular dynamics simulation of the vitreous silica surface. The Journal of
- 665 *Chemical Physics* **1983,** *78* (4), 2069-2072.
- 666 65. Stebbins, J. F.; McMillan, P., Compositional and temperature effects on five-coordinated silicon
- in ambient pressure silicate glasses. *Journal of Non-Crystalline Solids* **1993,** *160* (1), 116-125.
- 668 66. Sneh, O.; George, S. M., Thermal stability of hydroxyl groups on a well-defined silica surface. The
- 669 *Journal of physical chemistry* **1995,** *99* (13), 4639-4647.
- 670 67. Zhuravlev, L., The surface chemistry of amorphous silica. Zhuravlev model. *Colloids and Surfaces*
- 671 A: Physicochemical and Engineering Aspects **2000**, 173 (1), 1-38.
- 672 68. Rückriem, M.; Inayat, A.; Enke, D.; Gläser, R.; Einicke, W.-D.; Rockmann, R., Inverse gas
- 673 chromatography for determining the dispersive surface energy of porous silica. *Colloids and Surfaces A:*
- 674 Physicochemical and Engineering Aspects **2010**, 357 (1), 21-26.
- 675 69. Mahadik, D.; Rao, A. V.; Parale, V.; Kavale, M.; Wagh, P.; Ingale, S.; Gupta, S. C., Effect of surface
- 676 composition and roughness on the apparent surface free energy of silica aerogel materials. *Applied*
- 677 *Physics Letters* **2011,** *99* (10), 104104.
- 678 70. Kerisit, S.; Cooke, D. J.; Spagnoli, D.; Parker, S. C., Molecular dynamics simulations of the
- 679 interactions between water and inorganic solids. Journal of Materials Chemistry 2005, 15 (14), 1454-
- 680 1462.

- 681 71. Mkhonto, D.; de Leeuw, N. H., A computer modelling study of the effect of water on the surface
- structure and morphology of fluorapatite: introducing a Ca 10 (PO 4) 6 F 2 potential model. Journal of
- 683 *Materials Chemistry* **2002,** *12* (9), 2633-2642.
- de Leeuw, N. H.; Parker, S. C., Surface–water interactions in the dolomite problem. *Physical*
- 685 Chemistry Chemical Physics **2001**, 3 (15), 3217-3221.
- 73. Teleman, O.; Jönsson, B.; Engström, S., A molecular dynamics simulation of a water model with
- intramolecular degrees of freedom. *Molecular Physics* **1987**, *60* (1), 193-203.
- 688 74. Mahadevan, T.; Garofalini, S., Dissociative water potential for molecular dynamics simulations.
- 689 The Journal of Physical Chemistry B **2007**, 111 (30), 8919-8927.
- 690 75. De Leeuw, N.; Parker, S., Molecular-dynamics simulation of MgO surfaces in liquid water using a
- shell-model potential for water. *Physical Review B* **1998**, *58* (20), 13901.
- 692 76. Ben-Naim, A.; Marcus, Y., Solvation thermodynamics of nonionic solutes. *The Journal of*
- 693 chemical physics **1984**, 81 (4), 2016-2027.
- 694 77. Dickinson, J.; Langford, S.; Jensen, L.; McVay, G.; Kelso, J.; Pantano, C., Fractoemission from
- 695 fused silica and sodium silicate glasses. Journal of Vacuum Science & Technology A: Vacuum, Surfaces,
- 696 and Films **1988**, 6 (3), 1084-1089.
- 697 78. Kelso, J.; Pantano, C.; Garofalini, S., A comparison of ion scattering spectra and molecular
- dynamics simulations at the surface of silicate glasses. Surface science 1983, 134 (3), L543-L549.
- 699 79. Langford, S.; Jensen, L.; Dickinson, J.; Pederson, L., Alkali emission accompanying fracture of
- sodium silicate glasses. *Journal of Materials Research* **1991**, *6* (06), 1358-1368.